OPTIMIZED SCHWARZ METHODS WITH NONOVERLAPPING CIRCULAR DOMAIN DECOMPOSITION

MARTIN J. GANDER AND YINGXIANG XU

ABSTRACT. While the classical Schwarz method can only be used with overlap, optimized Schwarz methods can also be used without overlap, which can be an advantage when simulating heterogeneous problems, problems with jumping coefficients, or also for independent mesh generation per subdomain. The analysis of nonoverlapping optimized Schwarz methods has so far been restricted to the case of straight interfaces, even though the method has been successfully used with curved interfaces. We close this gap by presenting a rigorous analysis of optimized Schwarz methods for circular domain decompositions. We derive optimized zeroth and second order transmission conditions for a model elliptic operator in two dimensions, and show why the straight interface analysis results, when properly scaled to include the curvature, are also successful for curved interfaces. Our analysis thus complements earlier asymptotic results by Lui for curved interfaces, where the influence of the curvature remained unknown. We illustrate our results with numerical experiments.

1. INTRODUCTION

With the arrival of exascale computing, domain decomposition (DD) methods are the main focus of interest for the large scale parallel solution of partial differential equations. Among modern DD methods, optimized Schwarz methods (OSMs), which use transmission conditions based on an optimization procedure, have been successfully used in many application areas, e.g. for Maxwell's equations [10, 13, 38, 39, 41], Helmholtz problems [7, 12, 25, 35, 42], Navier-Stokes equations [9], advection diffusion problems [8, 23, 36, 40], wave equations [22, 24], and even in circuit simulation [3, 4, 20]. The underlying structure which makes optimized Schwarz methods work has also been rediscovered more recently under various names; see for example the sweeping preconditioner [2, 16, 26, 27, 42] and the source transfer method [11].

Optimized Schwarz methods are usually analyzed for a model problem with straight interfaces using Fourier techniques (see [18] and references therein), and the optimized transmission parameters are given in closed form asymptotically in terms of the mesh parameter or the overlap size and the problem parameters. In most applications however the computational domain is decomposed according to physical properties or by partitioning software, and hence the artificial interfaces
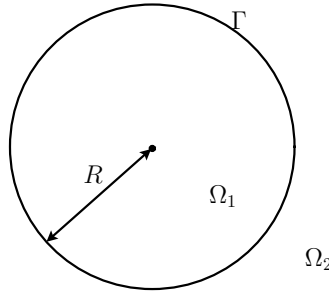
FIGURE 1. The nonoverlapping circular domain decomposition used.

are seldom flat. Nevertheless numerical experiments for many applications have shown that the optimized transmission parameters from the straight interface analysis also work well for curved interfaces; see for example [18, 25, 35]. Optimized Schwarz methods for overlapping circular decompositions have been studied in [28]. For a nonoverlapping optimized Schwarz method with nonstraight interfaces, spectral estimates of Poincaré-Steklov operators confirmed the asymptotic behavior of optimized transmission conditions in the mesh size (see [32, 33]), but the precise dependence on the constants and the interface curvature could not be captured.

While the overlap in general accelerates the convergence of optimized Schwarz methods [18], nonoverlapping variants have advantages for problems with jumping coefficients [14, 15, 21], heterogeneous media [34] and also certain interface problems [43]. We study in this paper optimized Schwarz methods for a nonoverlapping circular domain decomposition. The results have many potential applications, e.g. to problems with domains that are circular, circular sectors or circular rings, for example fluid-structure interaction problems [31, 37]. We will also show how the interface curvature for a general interface can be included in the optimized transmission conditions in a heuristic fashion.

We consider the model problem

$$(1.1) \qquad\qquad (\Delta - \eta)u = f, \quad \text{on } \Omega = \mathbb{R}^2,$$

with the model parameter $\eta > 0$. The domain Ω is decomposed into the two subdomains

$$(1.2) \qquad \Omega_1 = \{(x,y)|\sqrt{x^2+y^2} < R\}, \quad \Omega_2 = \{(x,y)|R < \sqrt{x^2+y^2}\},$$

such that $\Omega = \bar{\Omega}_1 \cup \bar{\Omega}_2$ (see Figure 1), with the interface $\Gamma := \bar{\Omega}_1 \cap \bar{\Omega}_2 = \{(x,y)|\sqrt{x^2+y^2} = R\}$. In polar coordinates, the model problem (1.1) reads

$$(1.3) \qquad\qquad \partial_{rr}u + \frac{1}{r}\partial_r u + \frac{1}{r^2}\partial_{\theta\theta}u - \eta u = f.$$

A parallel Schwarz algorithm for (1.3) with subdomains Ω_1 and Ω_2 solves for $n = 1, 2, \ldots$

$$(1.4) \qquad \begin{aligned} \partial_{rr}u_1^n + \frac{1}{r}\partial_r u_1^n + \frac{1}{r^2}\partial_{\theta\theta}u_1^n - \eta u_1^n &= f \text{ in } \Omega_1, \\ \partial_{rr}u_2^n + \frac{1}{r}\partial_r u_2^n + \frac{1}{r^2}\partial_{\theta\theta}u_2^n - \eta u_2^n &= f \text{ in } \Omega_2, \end{aligned}$$

with the transmission conditions

$$(1.5) \qquad \mathcal{B}_1(u_1^n) = \mathcal{B}_1(u_2^{n-1}), \quad \mathcal{B}_2(u_2^n) = \mathcal{B}_2(u_1^{n-1}), \quad \text{on } \Gamma,$$

where $\mathcal{B}_1$ and $\mathcal{B}_2$ are transmission operators to be chosen such that the subdomain problems are well posed and the method converges as fast as possible. With the classical choice of Dirichlet transmission conditions, i.e. $\mathcal{B}_i = I$ the identity operator, the Schwarz method without overlap would not converge, so more effective transmission conditions are needed.

2. Optimized Schwarz algorithms

Choosing $\mathcal{B}_i(u) = \partial_r u + \mathcal{S}_i u$ in (1.5), we obtain

$$(2.1) \qquad \begin{aligned} (\partial_r + \mathcal{S}_1)u_1^n(R,\theta) &= (\partial_r + \mathcal{S}_1)u_2^{n-1}(R,\theta), \\ (\partial_r + \mathcal{S}_2)u_2^n(R,\theta) &= (\partial_r + \mathcal{S}_2)u_1^{n-1}(R,\theta), \end{aligned}$$

where $\theta \in [0, 2\pi)$ and $\mathcal{S}_i, i = 1, 2$, are linear operators along the interface in the θ direction, which we will determine in what follows to get the best possible performance of the Schwarz algorithm. By linearity, we only need to consider the error equations, i.e. the homogeneous case $f = 0$. Applying a Fourier transform to (1.4) in the θ direction for $f = 0$ gives

$$(2.2) \qquad \begin{aligned} \partial_{rr}\hat{u}_1^n + \frac{1}{r}\partial_r\hat{u}_1^n - \left(\frac{k^2}{r^2} + \eta\right)\hat{u}_1^n &= 0, \quad r < R, \quad k \in \mathbb{K}, \\ \partial_{rr}\hat{u}_2^n + \frac{1}{r}\partial_r\hat{u}_2^n - \left(\frac{k^2}{r^2} + \eta\right)\hat{u}_2^n &= 0, \quad r > R, \quad k \in \mathbb{K}, \end{aligned}$$

where $\mathbb{K} = [k_{\min}, k_{\max}]$ consists of the relevant frequencies involved in the computation. For a circular domain, the lowest frequency $k_{\min}$ can be estimated by 1 and the highest frequency $k_{\max}$ by π/h, where h is the angular mesh size along the interface. If the computational domain is a circular sector with the central angle α and homogeneous Dirichlet boundary condition on both radii, the lowest frequency $k_{\min}$ could be estimated by π/α, and the highest frequency again by π/h. Note that in the limit for an angle of $\alpha = 2\pi$, we get $k_{\min} = \frac{1}{2}$, which is correct for Dirichlet conditions and different from $k_{\min} = 1$ for the periodic case of the entire circular domain.

Taking also a Fourier transform of the transmission conditions (2.1) in the θ direction gives

$$(2.3) \qquad \begin{aligned} (\partial_r + \sigma_1(k))\hat{u}_1^n(R,k) &= (\partial_r + \sigma_1(k))\hat{u}_2^{n-1}(R,k), \quad k \in \mathbb{K}, \\ (\partial_r + \sigma_2(k))\hat{u}_2^n(R,k) &= (\partial_r + \sigma_2(k))\hat{u}_1^{n-1}(R,k), \quad k \in \mathbb{K}, \end{aligned}$$

where $\sigma_{1,2}(k)$ are the symbols of $\mathcal{S}_{1,2}$. We find from (2.2) the subdomain solutions in the Fourier transformed domain to be

$$(2.4) \qquad \hat{u}_1^n(r,k) = C_1^n(k)I_k(\sqrt{\eta}r), \quad \hat{u}_2^n(r,k) = C_2^n(k)K_k(\sqrt{\eta}r),$$

where $I_k(x)$ and $K_k(x)$ are the modified Bessel functions of the first and the second kind [1]. Inserting these solutions into the Fourier transformed transmission

conditions (2.3), we obtain by induction

$$(2.5) \qquad \hat{u}_1^{2n}(R,k) = \rho_{opt}^n \hat{u}_1^0(R,k), \qquad \hat{u}_2^{2n}(R,k) = \rho_{opt}^n \hat{u}_2^0(R,k),$$

where the convergence factor ρ_{opt} is given by

$$(2.6) \quad \rho_{opt}(k,R,\eta,\sigma_1(k),\sigma_2(k)) := \frac{\sqrt{\eta}v_k(\sqrt{\eta}R) + \sigma_1(k)}{\sqrt{\eta}w_k(\sqrt{\eta}R) + \sigma_1(k)} \cdot \frac{\sqrt{\eta}w_k(\sqrt{\eta}R) + \sigma_2(k)}{\sqrt{\eta}v_k(\sqrt{\eta}R) + \sigma_2(k)},$$

with $v_k(x) := \frac{K_k'(x)}{K_k(x)}$ and $w_k(x) := \frac{I_k'(x)}{I_k(x)}$. The following lemma about these functions can be found in [28].

Lemma 2.1. *For fixed $x > 0$, both $-v_k(x)$ and $w_k(x)$ are positive functions which are strictly increasing in k for $k \geq 0$. Moreover, $\lim_{k\to+\infty} -v_k(x) = \lim_{k\to+\infty} w_k(x) = +\infty$.*

Let $G_k(x) := w_k(x) - v_k(x)$. Then $G_k(x)$ is also strictly increasing in k for $k > 0$ by Lemma 2.1. The functions $v_k(x)$, $w_k(x)$ and $G_k(x)$ can be evaluated using the relations [1]

$$(2.7) \qquad I_k'(x) = \frac{1}{2}(I_{k-1}(x) + I_{k+1}(x)) = I_{k+1}(x) + \frac{k}{x}I_k(x),$$

$$(2.8) \qquad K_k'(x) = -\frac{1}{2}(K_{k-1}(x) + K_{k+1}(x)) = \frac{k}{x}K_k(x) - K_{k+1}(x).$$

Theorem 2.2 (Optimal Schwarz method). *If $\sigma_1(k) = -\sqrt{\eta}v_k(\sqrt{\eta}R)$ and $\sigma_2(k) = -\sqrt{\eta}w_k(\sqrt{\eta}R)$, the Schwarz algorithm described by (1.4) and (2.1) converges in two iterations.*

Proof. The proof is similar to Lemma 2.2 in [17]; see also [18]. □

Unfortunately, the optimal symbols $\sigma_i(k)$ described in Theorem 2.2 correspond to nonlocal operators $\mathcal{S}_i$, $i = 1, 2$ (see [18]), which are hard to implement and expensive to use. In optimized Schwarz methods, one uses local approximations of $\sigma_i(k)$, $i = 1, 2$. Here, we choose polynomials of degree two:

$$(2.9) \qquad \sigma_1^{app}(k) = p_1 + q_1 k^2, \quad \sigma_2^{app}(k) = -p_2 - q_2 k^2.$$

The transmission conditions with this polynomial approximation are

$$(2.10) \qquad \begin{aligned} (\partial_r + p_1 - q_1\partial_{\theta\theta})u_1^n &= (\partial_r + p_1 - q_1\partial_{\theta\theta})u_2^{n-1}, \\ (\partial_r - p_2 + q_2\partial_{\theta\theta})u_2^n &= (\partial_r - p_2 + q_2\partial_{\theta\theta})u_1^{n-1}. \end{aligned}$$

Inserting the approximation (2.9) into (2.6), the convergence factor of the parallel Schwarz algorithm described by (1.4) and (2.1) becomes
(2.11)

$$\rho(k,R,\eta,p_1,p_2,q_1,q_2) = \frac{-\sqrt{\eta}v_k(\sqrt{\eta}R) - p_1 - q_1 k^2}{\sqrt{\eta}w_k(\sqrt{\eta}R) + p_1 + q_1 k^2} \cdot \frac{\sqrt{\eta}w_k(\sqrt{\eta}R) - p_2 - q_2 k^2}{-\sqrt{\eta}v_k(\sqrt{\eta}R) + p_2 + q_2 k^2}.$$

Remark 2.3. Unlike the infinite domain decomposition case analyzed in [18], the parallel Schwarz methods (1.4) and (2.10) do not converge for all parameters $p_i > 0$ and $q_i \geq 0$, $i = 1, 2$. This was also observed in the overlapping circular domain decomposition case [28]. For example, the choice $p_1 = 0.01$, $p_2 = 100$, $q_1 = q_2 = 0$
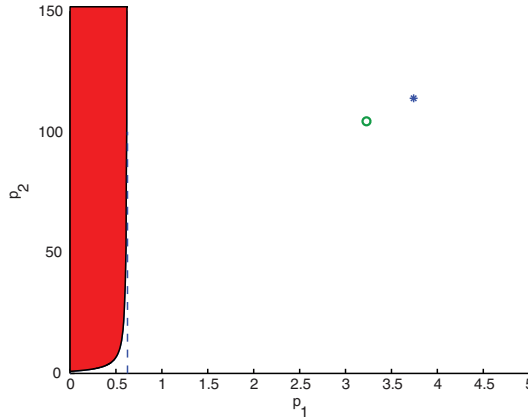
FIGURE 2. Domain in which the OSM with 2-sided Robin condition converges for $\eta = 2$, $R = 0.5$ and $h = 0.01$. The parameters outside the dark colored region lead to a convergent method (the vertical dashed line is the curve's asymptote). The star indicates the position of the optimized parameters from Theorem 2.12, and the circle the one obtained by equi-oscillation.

leads with the model parameter $\eta = 2$ and $R = 0.5$ to a convergence factor -1.214404261 at $k = 1$. The dark colored region in Figure 2 is the complement of the set of parameter choices which result in a convergent method. The Turán type inequalities (2.13) and (2.14) we will see later show that $-v_k(x) > w_k(x)$ for $k > 0$. Therefore, for $q_1 = q_2 = 0$ and p_1 small enough, the first factor in ρ will be bigger than one, $\frac{-\sqrt{\eta}v_k(\sqrt{\eta}R)-p_1}{\sqrt{\eta}w_k(\sqrt{\eta}R)+p_1} > 1$, and the second factor $\frac{\sqrt{\eta}w_k(\sqrt{\eta}R)-p_2}{-\sqrt{\eta}v_k(\sqrt{\eta}R)+p_2} \to -1$ as p_2 tends to infinity, which shows that this is the only case of divergence. It is thus better to use $p_1 > p_2$, which agrees with the results in [29].

Since the modified Bessel functions $I_k(x)$ and $K_k(x)$ are involved through $w_k(x)$ and $v_k(x)$, the convergence factor $\rho(k, R, \eta, p_1, p_2, q_1, q_2)$ in (2.11) cannot be optimized directly. We therefore propose the approximation

$$(2.12) \quad \rho_{app}(k, R, \eta, p_1, p_2, q_1, q_2) = \frac{\sqrt{\eta + \frac{k^2}{R^2}} - p_1 - q_1 k^2}{\sqrt{\eta + \frac{k^2}{R^2}} + p_1 + q_1 k^2} \frac{\sqrt{\eta + \frac{k^2}{R^2}} - p_2 - q_2 k^2}{\sqrt{\eta + \frac{k^2}{R^2}} + p_2 + q_2 k^2},$$

with the following estimate.

Theorem 2.4 (Approximation of the convergence factor). *For $k > 1$, there exists a constant $C > 0$ independent of k such that*

$$|\rho(k, R, \eta, p_1, p_2, q_1, q_2) - \rho_{app}(k, R, \eta, p_1, p_2, q_1, q_2)| \le \frac{C}{k^3}.$$

Proof. As Lemma 3.3 in [28], the proof is based on the Turán type inequalities (for a proof, see [5])

$$(2.13) \qquad \sqrt{\frac{k}{k+1}x^2 + k^2} < \frac{xI_k'(x)}{I_k(x)} < \sqrt{x^2 + k^2}, \qquad \forall x > 0, \ k > 0,$$

$$(2.14) \qquad -\sqrt{\frac{k}{k-1}x^2 + k^2} < \frac{xK_k'(x)}{K_k(x)} < -\sqrt{x^2 + k^2}, \qquad \forall x > 0, \ k > 1,$$

where the right hand side inequality in (2.14) holds for $k > 0$.

We consider first the case $p_1 + q_1 k^2 < -\sqrt{\eta} v_k(\sqrt{\eta}R)$ and $p_2 + q_2 k^2 < \sqrt{\eta} w_k(\sqrt{\eta}R)$. Using the Turán type inequalities (2.13) and (2.14) we arrive at

$$\rho \le \frac{\sqrt{\frac{k\eta}{k-1} + \frac{k^2}{R^2}} - p_1 - q_1 k^2}{\sqrt{\frac{k\eta}{k+1} + \frac{k^2}{R^2}} + p_1 + q_1 k^2} \cdot \frac{\sqrt{\eta + \frac{k^2}{R^2}} - p_2 - q_2 k^2}{\sqrt{\eta + \frac{k^2}{R^2}} + p_2 + q_2 k^2} = \rho_{app} + O(\frac{1}{k^3}).$$

Similarly, we obtain

$$\rho \ge \frac{\sqrt{\eta + \frac{k^2}{R^2}} - p_1 - q_1 k^2}{\sqrt{\eta + \frac{k^2}{R^2}} + p_1 + q_1 k^2} \cdot \frac{\sqrt{\frac{k\eta}{k+1} + \frac{k^2}{R^2}} - p_2 - q_2 k^2}{\sqrt{\frac{k\eta}{k-1} + \frac{k^2}{R^2}} + p_2 + q_2 k^2} = \rho_{app} + O(\frac{1}{k^3}).$$

Integrating the two inequalities above, we arrive at the assertion for the case $p_1 + q_1 k^2 < -\sqrt{\eta} v_k(\sqrt{\eta}R)$ and $p_2 + q_2 k^2 < \sqrt{\eta} w_k(\sqrt{\eta}R)$. For the other cases, the results can be obtained similarly. □

In the rest of this section, we study the influence of various choices of the free parameters $p_i > 0$, $q_i \ge 0$, $i = 1, 2$, on the performance of the optimized Schwarz method.

2.1. **Taylor transmission conditions.** A simple way to use information from the optimal symbols $\sigma_i(k)$ is to use a Taylor expansion. Since for k small

$$\sigma_1(k) = -\sqrt{\eta} v_0(\sqrt{\eta}R) + O(k), \quad \sigma_2(k) = -\sqrt{\eta} w_0(\sqrt{\eta}R) + O(k),$$

one can choose $p_1 = -\sqrt{\eta} v_0(\sqrt{\eta}R)$, $p_2 = \sqrt{\eta} w_0(\sqrt{\eta}R)$ and $q_1 = q_2 = 0$, which leads to the Taylor transmission condition of order 0 (T0). The corresponding Schwarz method has the convergence factor

$$(2.15) \qquad \rho_{T0}(k, R, \eta) = \frac{-v_k(\sqrt{\eta}R) + v_0(\sqrt{\eta}R)}{w_k(\sqrt{\eta}R) - v_0(\sqrt{\eta}R)} \cdot \frac{w_k(\sqrt{\eta}R) - w_0(\sqrt{\eta}R)}{-v_k(\sqrt{\eta}R) + w_0(\sqrt{\eta}R)},$$

where $v_0(\sqrt{\eta}R) = -\frac{K_1(\sqrt{\eta}R)}{K_0(\sqrt{\eta}R)}$ and $w_0(\sqrt{\eta}R) = \frac{I_1(\sqrt{\eta}R)}{I_0(\sqrt{\eta}R)}$ by the connection formulas (2.7) and (2.8). We show in Figure 3 the dependence of this convergence factor on k.

Theorem 2.5 (Taylor asymptotics). *The Schwarz method* (1.4) *with Taylor transmission condition of order* 0 *satisfies for* $k_{\max} \to +\infty$ *the convergence factor estimate*

$$\max_{0 \le k \le k_{\max}} |\rho_{T0}(k, R, \eta)| = 1 - 2\sqrt{\eta} R G_0(\sqrt{\eta}R) k_{\max}^{-1} + O(k_{\max}^{-2}).$$

Proof. By Lemma 2.1, it is easy to show that $\frac{w_k(\sqrt{\eta}R) - w_0(\sqrt{\eta}R)}{w_k(\sqrt{\eta}R) - v_0(\sqrt{\eta}R)}$ is positive and strictly increasing in k for $k > 0$. A similar result holds for $\frac{-v_k(\sqrt{\eta}R) + v_0(\sqrt{\eta}R)}{-v_k(\sqrt{\eta}R) + w_0(\sqrt{\eta}R)}$. Thus, as the product of these two, the convergence factor ρ_{T0} is positive and strictly
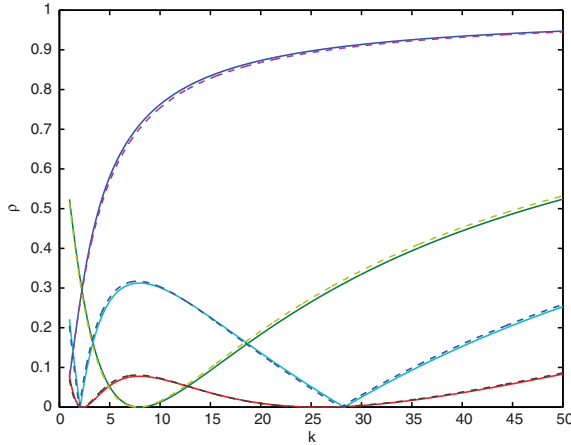
FIGURE 3. Convergence factors for $\eta = 2$ and $R = 0.5$ with various transmission conditions obtained from the circular interface analysis (solid), compared to those from the straight interface analysis [18] with the frequencies appropriately scaled (dashed). From top to bottom: T0, OO0, O2s and OO2.

increasing in k for $k > 0$. Hence the convergence factor ρ_{T0} attains its maximum at $k_{\max}$. Using Theorem 2.4 we thus obtain

$$
\begin{aligned}
\max_{0 \leq k \leq k_{\max}} |\rho_{T0}(k, R, \eta)| &= \rho_{T0}(k_{\max}, R, \eta) \\
&= \rho_{app}(k_{\max}, R, \eta, -\sqrt{\eta}v_0(\sqrt{\eta}R), \sqrt{\eta}w_0(\sqrt{\eta}R), 0, 0) + O(k_{\max}^{-3}) \\
&= 1 - 2\sqrt{\eta}R G_0(\sqrt{\eta}R)k_{\max}^{-1} + O(k_{\max}^{-2}). \qquad \square
\end{aligned}
$$

Note that one can also use a Taylor expansion about another frequency k, instead of $k = 0$, which would lead to transmission conditions that are very effective for that particular frequency. An example can be seen in Figure 3, the second curve (green) from the top. We will show in the next section that there is an optimal choice for the frequency about which to expand by reinterpreting the problem as an optimization problem for a Robin transmission condition. Also higher order Taylor conditions can be obtained in principle by expanding the optimal choices $\sigma_1(k)$ and $\sigma_2(k)$ in k to higher orders. However, the derivatives of the modified Bessel functions $I_k(x)$ and $K_k(x)$ in k are not easy to obtain [1], so in what follows we focus on optimized transmission conditions instead.

2.2. **Optimized Robin transmission conditions.** From Figure 3 and the above analysis, we see that the Taylor transmission condition is only efficient in damping low frequency errors. To balance the damping on each frequency mode, the parameters in the transmission conditions should be determined by solving the min-max problem

$$
(2.16) \qquad \min_{p_i > 0, q_i \geq 0} \max_{k \in \mathbb{K}} |\rho(k, R, \eta, p_1, p_2, q_1, q_2)|.
$$

Solving (2.16) with different constraints on the free parameters will lead to Schwarz methods with different optimized transmission conditions.

We consider first the restriction $p_1 = p_2 = p$, $q_1 = q_2 = 0$, which leads to the simplified convergence factor

$$\rho_{OO0}(k, R, \eta, p) = \frac{-\sqrt{\eta}v_k(\sqrt{\eta}R) - p}{-\sqrt{\eta}v_k(\sqrt{\eta}R) + p} \cdot \frac{\sqrt{\eta}w_k(\sqrt{\eta}R) - p}{\sqrt{\eta}w_k(\sqrt{\eta}R) + p},$$

where the parameter p should be determined by solving the min-max problem

$$(2.17) \qquad\qquad \min_{p>0} \max_{k \in \mathbb{K}} |\rho_{OO0}(k, R, \eta, p)|.$$

The resulting transmission condition is known as the optimized transmission condition of order 0 (OO0). We first need a lemma, which will also be useful in subsection 2.4.

Lemma 2.6. *Let $k_0(p)$ be the positive solution of* $\min\{-\sqrt{\eta}v_k(\sqrt{\eta}R), \sqrt{\eta}w_k(\sqrt{\eta}R)\}$ $= p$. *Then $k_0(p) \sim pR$ for $p \to +\infty$. In addition, the result holds as well if 'min' is replaced by 'max'.*

Proof. Based on the Turán type inequalities (2.13) and (2.14), we only need to show the result for the following cases:

- $\sqrt{\eta + \frac{k^2}{R^2}} = p$: expanding the solution $k_0(p) = \sqrt{p^2 - \eta}R$ in p for p large gives the desired result.
- $\sqrt{\frac{k}{k+1}\eta + \frac{k^2}{R^2}} = p$: squaring on both sides and inserting the ansatz $k := C_k p^\alpha$, $\alpha > 0$, we obtain $\eta - \frac{\eta}{C_k p^\alpha + 1} + \frac{C_k^2 p^{2\alpha}}{R^2} = p^2$. Since the equation should hold for any p large, we arrive at the desired result by setting the leading terms on both sides equal.
- $\sqrt{\frac{k}{k-1}\eta + \frac{k^2}{R^2}} = p$: the proof is similar to the case above. $\qquad\square$

Theorem 2.7 (Optimized Robin parameter). *The solution p^* to the min-max problem (2.17) is given in closed form by*

$$(2.18) \quad p^* = \sqrt{\eta} \left(\frac{v_{k_{\min}}^* w_{k_{\min}}^* v_{k_{\max}}^* w_{k_{\max}}^* \left(-\frac{1}{v_{k_{\max}}^*} + \frac{1}{w_{k_{\max}}^*} + \frac{1}{v_{k_{\min}}^*} - \frac{1}{w_{k_{\min}}^*} \right)}{-v_{k_{\min}}^* + w_{k_{\min}}^* + v_{k_{\max}}^* - w_{k_{\max}}^*} \right)^{\frac{1}{2}},$$

where $v_k^* = v_k(\sqrt{\eta}R)$ and $w_k^* = w_k(\sqrt{\eta}R)$. In addition, the optimized parameter p^* behaves asymptotically like $p^* = 2^{-\frac{1}{2}} \eta^{\frac{1}{4}} G_{\min}^{\frac{1}{2}} R^{-\frac{1}{2}} k_{\max}^{\frac{1}{2}}$ as $k_{\max} \to +\infty$ with $G_{\min} = G_{k_{\min}}(\sqrt{\eta}R)$.

Proof. We separate the proof into the following three steps.

In the first step we show that increasing p decreases $\rho_{OO0}(k, R, \eta, p)$ for all $k \geq k_{\min}$ if $p \leq \sqrt{-\eta v_{k_{\min}}(\sqrt{\eta}R) w_{k_{\min}}(\sqrt{\eta}R)}$, which implies that one only needs to consider the problem for $p > \sqrt{-\eta v_{k_{\min}}(\sqrt{\eta}R) w_{k_{\min}}(\sqrt{\eta}R)}$. This result follows directly from the fact that, for fixed $k \geq k_{\min}$, the convergence factor $\rho_{OO0}(k, R, \eta, p)$ attains its unique minimum at $\bar{p} = \sqrt{-\eta v_k(\sqrt{\eta}R) w_k(\sqrt{\eta}R)}$, a value that is greater than or equal to $\sqrt{-\eta v_{k_{\min}}(\sqrt{\eta}R) w_{k_{\min}}(\sqrt{\eta}R)}$ by Lemma 2.1.

In the second step, we show that $\max_{k \in [k_{\min}, k_1(p)) \cup (k_2(p), k_{\max}]} |\rho_{OO0}(k, R, \eta, p)|$ achieves its minimum if

(2.19) $$\rho_{OO0}(k_{\min}, R, \eta, p) = \rho_{OO0}(k_{\max}, R, \eta, p),$$

where $k_{1,2}(p)$ are solutions of $-\sqrt{\eta} v_k(\sqrt{\eta}R) = p$ and $\sqrt{\eta} w_k(\sqrt{\eta}R) = p$ respectively which satisfy $k_1(p) < k_2(p)$ by the Turán type inequalities (2.13) and (2.14). When $k \in (k_{\min}, k_1(p))$, we have by Lemma 2.1 that both $\frac{-\sqrt{\eta} v_k(\sqrt{\eta}R) - p}{-\sqrt{\eta} v_k(\sqrt{\eta}R) + p}$ and $\frac{\sqrt{\eta} w_k(\sqrt{\eta}R) - p}{\sqrt{\eta} w_k(\sqrt{\eta}R) + p}$ are negative and increasing in k, which implies that ρ_{OO0}, as the product of these two, is positive and decreases in k for $k \in (k_{\min}, k_1(p))$. Similarly, we find that ρ_{OO0} is positive and increases in k for $k \in (k_2(p), k_{\max})$. In addition, with increasing p, $\rho_{OO0}(k_{\min}, R, \eta, p)$ increases and $\rho_{OO0}(k_{\max}, R, \eta, p)$ decreases. Based on this, we arrive at our assertion of this step. Consequently, solving (2.19) leads to (2.18), and a series expansion of p^* for $k_{\max}$ large gives the asymptotic behavior of p^*.

In the last step we show that $\max_{k_1(p^*) \leq k \leq k_2(p^*)} |\rho_{OO0}(k, R, \eta, p)|$ remains below the maximum value obtained previously. By Lemma 2.6 we have asymptotically $k_1(p^*) = 2^{-\frac{1}{2}} \eta^{\frac{1}{4}} G_{\min}^{\frac{1}{2}} R^{\frac{1}{2}} k_{\max}^{\frac{1}{2}}$. Using the convergence factor approximation in Theorem 2.4, we can conclude the proof, noting that for $k \in [k_1(p^*), k_2(p^*)]$,

$$\rho_{OO0}(k, R, \eta, p^*) = \rho_{app}(k, R, \eta, p^*, p^*, 0, 0) + O(k_{\max}^{-\frac{3}{2}}) = O(k_{\max}^{-\frac{3}{2}}). \qquad \square$$

Theorem 2.8 (Robin asymptotics)**.** *The Schwarz method* (1.4) *with optimized Robin condition has for* $k_{\max} \to +\infty$ *the asymptotic convergence factor estimate*

$$\max_{k \in \mathbb{K}} |\rho_{OO0}(k, R, \eta, p^*)| = 1 - 2^{\frac{3}{2}} \eta^{\frac{1}{4}} G_{\min}^{\frac{1}{2}} R^{\frac{1}{2}} k_{\max}^{-\frac{1}{2}} + O(k_{\max}^{-1}).$$

Proof. Using Theorem 2.7, it suffices to expand $\rho_{OO0}(k_{\min}, R, \eta, p^*)$ in $k_{\max}$. $\qquad \square$

2.3. **Optimized second order transmission condition.** We now restrict the free parameters to $p_1 = p_2 = p$, $q_1 = q_2 = q$, which gives the optimized transmission condition of order 2 (OO2), and the convergence factor (2.11) simplifies to

(2.20) $$\rho_{OO2}(k, R, \eta, p, q) = \frac{-\sqrt{\eta} v_k(\sqrt{\eta}R) - p - qk^2}{-\sqrt{\eta} v_k(\sqrt{\eta}R) + p + qk^2} \cdot \frac{\sqrt{\eta} w_k(\sqrt{\eta}R) - p - qk^2}{\sqrt{\eta} w_k(\sqrt{\eta}R) + p + qk^2}.$$

The free parameters p and q can then be determined by solving the min-max problem

(2.21) $$\min_{p>0, q \geq 0} \max_{k \in \mathbb{K}} |\rho_{OO2}(k, R, \eta, p, q)|.$$

We will need the following lemma.

Lemma 2.9. *Let* $\underline{k}_2(p, q) > \underline{k}_1(p, q)$ *be the positive solutions of*

$$\min\{-\sqrt{\eta} v_k(\sqrt{\eta}R), \sqrt{\eta} w_k(\sqrt{\eta}R)\} = p + qk^2$$

with $p = C_p k_{\max}^{\alpha}$ *and* $q = C_q k_{\max}^{-\beta}$, *where* $\beta > \alpha > 0$. *Then* $\underline{k}_{1,2}(p, q)$ *behave asymptotically for* $k_{\max} \to +\infty$ *like*

$$\underline{k}_1(p, q) = C_p R k_{\max}^{\alpha}, \quad \underline{k}_2(p, q) = C_q^{-1} R^{-1} k_{\max}^{\beta}.$$

Proof. From the proof of Lemma 2.6, we know $\min\{-\sqrt{\eta}v_k(\sqrt{\eta}R), \sqrt{\eta}u_k(\sqrt{\eta}R)\}$ behaves like $\frac{k}{R}$ for k large enough. Thus, we need to solve asymptotically the equation $Rqk^2 - k + Rp = 0$. Assuming that the solution is of the form $k = C_k k_{\max}^\gamma$, and inserting this assumption and the expressions for p and q, we get

$$\frac{C_k k_{\max}^\gamma}{R} - C_p k_{\max}^\alpha + C_q C_k^2 k_{\max}^{2\gamma-\beta} = 0.$$

If $\gamma \le \alpha$, we have $2\gamma - \beta < \gamma$ because $\alpha < \beta$. We then set the leading terms in the above equation equal to obtain $\gamma = \alpha$ and $C_k = RC_p$, which gives the solution $\underline{k}_1(p,q)$. Otherwise, if $\gamma > \alpha$, we set the leading terms in the above equation again equal to obtain $\gamma = \beta$ and $C_k = \frac{1}{RC_q}$, which gives the solution $\underline{k}_2(p,q)$. $\square$

Theorem 2.10 (Optimized second order parameters). *The parameters*

$$(2.22) \qquad p^* = 2^{-\frac{5}{4}}\eta^{\frac{3}{8}}G_{\min}^{\frac{3}{4}}R^{-\frac{1}{4}}k_{\max}^{\frac{1}{4}}, \qquad q^* = 2^{-\frac{1}{4}}\eta^{-\frac{1}{8}}G_{\min}^{-\frac{1}{4}}R^{-\frac{5}{4}}k_{\max}^{-\frac{3}{4}}$$

solve asymptotically the equi-oscillation equations

$$(2.23) \qquad \rho_{OO2}(k_{\min}, R, \eta, p, q) = \rho_{OO2}(\bar{k}^*, R, \eta, p, q) = \rho_{OO2}(k_{\max}, R, \eta, p, q),$$

with $\bar{k}^*$ given asymptotically by $\bar{k}^* = 2^{-\frac{1}{2}}\eta^{\frac{1}{4}}G_{\min}^{\frac{1}{2}}R^{\frac{1}{2}}k_{\max}^{\frac{1}{2}}$, at which $\rho_{app}(k, R, \eta, p, p, q, q)$ attains its unique interior maximum asymptotically.

Proof. First, it is easy to show that $\rho_{app}(k, R, \eta, p, p, q, q)$ attains its unique interior maximum at the point $\bar{k} = \bar{k}(p,q) := \sqrt{p/q - 2\eta R^2}$. If we make the ansatz $p := C_p k_{\max}^{\frac{1}{4}}$, $q := C_q k_{\max}^{-\frac{3}{4}}$, then $\bar{k}$ behaves like $\sqrt{C_p/C_q}k_{\max}^{\frac{1}{2}}$. Inserting the ansatz also into $\rho_{OO2}(k_{\min}, R, \eta, p, q)$ and expanding asymptotically in $k_{\max}$ gives

$$(2.24) \qquad \rho_{OO2}(k_{\min}, R, \eta, p, q) = 1 - \frac{2\eta^{\frac{1}{2}}G_{\min}}{C_p}k_{\max}^{-\frac{1}{4}} + O(k_{\max}^{-\frac{1}{2}}).$$

Inserting $\bar{k} = \sqrt{C_p/C_q}k_{\max}^{\frac{1}{2}}$ and the ansatz into $\rho_{app}(\bar{k}, R, \eta, p, p, q, q)$ and expanding asymptotically for $k_{\max}$ gives

$$\rho_{app}(\bar{k}, R, \eta, p, p, q, q) = 1 - 8\sqrt{C_p C_q}R k_{\max}^{-\frac{1}{4}} + O(k_{\max}^{-\frac{1}{2}}).$$

Thus, by Theorem 2.4 we have

$$(2.25) \qquad \begin{aligned} \rho_{OO2}(\bar{k}, R, \eta, p, q) &= \rho_{app}(\bar{k}, R, \eta, p, p, q, q) + O(k_{\max}^{-\frac{3}{2}}) \\ &= 1 - 8\sqrt{C_p C_q}R k_{\max}^{-\frac{1}{4}} + O(k_{\max}^{-\frac{1}{2}}). \end{aligned}$$

Inserting the ansatz also into $\rho_{app}(k_{\max}, R, \eta, p, p, q, q)$ and expanding asymptotically in $k_{\max}$ gives

$$\rho_{app}(k_{\max}, R, \eta, p, p, q, q) = 1 - \frac{4}{C_q R}k_{\max}^{-\frac{1}{4}} + O(k_{\max}^{-\frac{1}{2}}).$$

Again, using Theorem 2.4 we obtain

$$(2.26) \qquad \begin{aligned} \rho_{OO2}(k_{\max}, R, \eta, p, q) &= \rho_{app}(k_{\max}, R, \eta, p, p, q, q) + O(k_{\max}^{-3}) \\ &= 1 - \frac{4}{C_q R}k_{\max}^{-\frac{1}{4}} + O(k_{\max}^{-\frac{1}{2}}). \end{aligned}$$

From (2.23), we see that for any $k_{\max}$ large enough, the three results (2.24), (2.25) and (2.26) should be equal. We then just set the coefficients of the term $k_{\max}^{-\frac{1}{4}}$ in (2.24), (2.25) and (2.26) equal to obtain

$$\frac{2\eta^{\frac{1}{2}}G_{\min}}{C_p} = 8\sqrt{C_p C_q}R = \frac{4}{C_q R}.$$

The solution is $C_p^* = 2^{-\frac{5}{4}}\eta^{\frac{3}{8}}G_{\min}^{\frac{3}{4}}R^{-\frac{1}{4}}$, $C_q^* = 2^{-\frac{1}{4}}\eta^{-\frac{1}{8}}G_{\min}^{-\frac{1}{4}}R^{-\frac{5}{4}}$, which leads to (2.22), and the asymptotic expression of $\bar{k}^*$. □

Theorem 2.11 (OO2 asymptotics). *The parameters p^* and q^* given in (2.22) solve asymptotically the min-max problem (2.21), and the asymptotic convergence factor of the Schwarz method with optimized second order transmission condition for $k_{\max} \to +\infty$ is given by*

$$(2.27) \qquad \max_{k \in \mathbb{K}} |\rho_{OO2}(k, R, \eta, p^*, q^*)| = 1 - 2^{\frac{9}{4}}\eta^{\frac{1}{8}}G_{\min}^{\frac{1}{4}}R^{\frac{1}{4}}k_{\max}^{-\frac{1}{4}} + O(k_{\max}^{-\frac{1}{2}}).$$

Proof. We use three steps as well to prove this result.

First, we show that when $(p, q) = (p^*, q^*)$ the convergence factor $\rho_{OO2}(k, R, \eta, p, q)$ has only three local maxima at $k_{\min}$, $\bar{k}^*$ and $k_{\max}$. To this end, we denote $T_1(k, p, q)$ $:= \frac{-\sqrt{\eta}v_k(\sqrt{\eta}R)-p-qk^2}{-\sqrt{\eta}v_k(\sqrt{\eta}R)+p+qk^2}$ and $T_2(k, p, q) := \frac{\sqrt{\eta}w_k(\sqrt{\eta}R)-p-qk^2}{\sqrt{\eta}w_k(\sqrt{\eta}R)+p+qk^2}$. By Lemma 2.1 we know that both $-v_k(x)$ and $w_k(x)$ are increasing in k for $x > 0$ fixed. Since $T_1(k, p^*, q^*) < 0$ and $T_2(k, p^*, q^*) < 0$ for $k < \underline{k}_1(p^*, q^*)$ (for the definition of $\underline{k}_1(p, q)$, see Lemma 2.9), we obtain that both $T_1(k, p^*, q^*)$ and $T_2(k, p^*, q^*)$ are negative and increasing in k for $k < \underline{k}_1(p^*, q^*)$. Hence, $\rho_{OO2}(k, R, \eta, p^*, q^*)$, as the product of $T_{1,2}(k, p^*, q^*)$, decreases in k for $k < \underline{k}_1(p^*, q^*)$. Thus, $k_{\min}$ is a possible maximum point of $\rho_{OO2}(k, R, \eta, p^*, q^*)$. By Lemma 2.9 we know that $\underline{k}_1(p^*, q^*)$ behaves asymptotically like $\underline{k}_1(p^*, q^*) = Rp^* = 2^{-\frac{5}{4}}\eta^{\frac{3}{8}}G_{\min}^{\frac{3}{4}}R^{\frac{3}{4}}k_{\max}^{\frac{1}{4}}$; therefore when $k > \underline{k}_1(p^*, q^*)$ we have $\rho_{OO2}(k, R, \eta, p^*, q^*) = \rho_{app}(k, R, \eta, p^*, p^*, q^*, q^*) + O(k_{\max}^{-\frac{3}{4}})$. Now it is easy to show that $\rho_{app}(k, R, \eta, p^*, p^*, q^*, q^*)$ has local maxima for $k > \underline{k}_1$ only at $\bar{k} = 2^{-\frac{1}{2}}\eta^{\frac{1}{4}}G_{\min}^{\frac{1}{2}}R^{\frac{1}{2}}k_{\max}^{\frac{1}{2}}$ and $k_{\max}$, and thus also $\rho_{OO2}(k, R, \eta, p^*, q^*)$ has only two further local maxima at $\bar{k}$ and $k_{\max}$.

Next, we calculate the maximum of $\rho_{OO2}(k, R, \eta, p^*, q^*)$. Due to (2.23), we evaluate directly $\rho_{OO2}(k, R, \eta, p^*, q^*)$ at $k_{\min}$ with parameters p^* and q^* from (2.22) to obtain

$$\rho_{OO2}(k_{\min}, R, \eta, p^*, q^*) = 1 - 2^{\frac{9}{4}}\eta^{\frac{1}{8}}G_{\min}^{\frac{1}{4}}R^{\frac{1}{4}}k_{\max}^{-\frac{1}{4}} + O(k_{\max}^{-\frac{1}{2}}).$$

To show that p^* and q^* from (2.22) solve asymptotically the min-max problem (2.21), we finally need to show that any parameters (p, q) other than (p^*, q^*) would lead at some k^* to a convergence factor $\rho_{OO2}(k, R, \eta, p, q)$ that is larger than $\rho_{OO2}(k_{\min}, R, \eta, p^*, q^*)$ asymptotically. To this end, we denote $p := C_p k_{\max}^{\alpha}$ and $q := C_q k_{\max}^{-\beta}$, and similarly $p^* := C_p^* k_{\max}^{\alpha^*}$ and $q^* := C_q^* k_{\max}^{-\beta^*}$ with $\alpha^* = \frac{1}{4}$, $\beta^* = \frac{3}{4}$. We then try to find a k^* such that when $(p, q) \neq (p^*, q^*)$, the asymptotic performance is worse for $k_{\max}$ large enough:

$$\rho_{OO2}(k^*, R, \eta, p, q) > 1 - \frac{2\eta^{\frac{1}{2}}G_{\min}}{C_p^*}k_{\max}^{-\frac{1}{4}}.$$

We first show that if $(\alpha, \beta) \neq (\alpha^*, \beta^*)$, then the asymptotic order of the resulting optimized Schwarz method is worse. To do so, it suffices to analyze the following five cases:

a) $\alpha > \alpha^*$, $\beta > -\alpha$. In this case at $k^* = k_{\min}$ we have $\rho_{OO2}(k_{\min}, R, \eta, p, q) = 1 - \frac{2\sqrt{\eta}G_{\min}}{C_p}k_{\max}^{-\alpha} + O(k_{\max}^{-2\alpha})$.

b) $\alpha > \alpha^*$, $\beta < -\alpha$. In this case at $k^* = k_{\min}$ we have $\rho_{OO2}(k_{\min}, R, \eta, p, q) = 1 - 2\sqrt{\eta}\frac{G_{\min}}{C_q k_{\min}^2}k_{\max}^{\beta} + o(k_{\max}^{\beta})$.

c) $-\beta = \alpha > \alpha^*$. In this case at $k^* = k_{\min}$ we have $\rho_{OO2}(k_{\min}, R, \eta, p, q) = 1 - \frac{2\sqrt{\eta}G_{\min}}{C_p + C_q k_{\min}^2}k_{\max}^{\alpha} + o(k_{\max}^{\alpha})$.

d) $\alpha \leq \alpha^*$, $\beta \geq \beta^*$ but $(\alpha, \beta) \neq (\alpha^*, \beta^*)$. In this case at $k^* = C_k k_{\max}^{\frac{\alpha+\beta}{2}}$ we have $\rho_{OO2}(k^*, R, \eta, p, q) = 1 - 4\frac{C_p + C_q C_k^2}{C_k}R k_{\max}^{-\frac{\beta-\alpha}{2}} + o(k_{\max}^{-\frac{\beta-\alpha}{2}})$.

e) $\alpha \leq \alpha^*$, $\beta < \beta^*$. In this case at $k^* = k_{\max}$ we have $\rho_{OO2}(k^*, R, \eta, p, q) = 1 - 4\frac{1}{C_q R}k_{\max}^{\beta-1} + o(k_{\max}^{\beta-1})$.

In each of these cases, we see that at k^* the convergence factor $\rho_{OO2}(k^*, R, \eta, p, q)$ behaves asymptotically like $1 - Ck_{\max}^{-\delta}$ with $\delta > \frac{1}{4}$, and thus the method is asymptotically worse than with the choice $(\alpha, \beta) = (\alpha^*, \beta^*)$. We now consider the case $(\alpha, \beta) = (\alpha^*, \beta^*)$ but $(C_p, C_q) \neq (C_p^*, C_q^*)$. From (2.24) we see that if $C_p > C_p^*$ and $k_{\max}$ is large enough, we have $\rho_{OO2}(k_{\min}, R, \eta, p, q) > \rho_{OO2}(k_{\min}, R, \eta, p^*, q^*)$. If $C_q > C_q^*$ and $k_{\max}$ is large enough, we have from (2.26) that $\rho_{OO2}(k_{\max}, R, \eta, p, q) > \rho_{OO2}(k_{\max}, R, \eta, p^*, q^*)$. Finally, from (2.25) we see that if $C_p < C_p^*$ or $C_q < C_q^*$ and $k_{\max}$ is large enough, then $\rho_{OO2}(\bar{k}, R, \eta, p, q) > \rho_{OO2}(\bar{k}, R, \eta, p^*, q^*)$, which concludes the proof. $\square$

2.4. **Optimized two-sided Robin transmission condition.** If we restrict the free parameters to the set $p_1 > 0$, $p_2 > 0$, $q_1 = q_2 = 0$, we obtain an optimized two-sided Robin transmission condition (O2s); i.e. we use different transmission parameters on each side of the interface. The convergence factor (2.11) can then be simplified to

$$(2.28) \qquad \rho_{O2s}(k, R, \eta, p_1, p_2) = \frac{-\sqrt{\eta}v_k(\sqrt{\eta}R)-p_1}{\sqrt{\eta}w_k(\sqrt{\eta}R)+p_1} \cdot \frac{\sqrt{\eta}w_k(\sqrt{\eta}R)-p_2}{-\sqrt{\eta}v_k(\sqrt{\eta}R)+p_2}.$$

The free parameters p_1 and p_2 are determined by solving the min-max problem

$$(2.29) \qquad \min_{p_1, p_2 > 0} \max_{k \in \mathbb{K}} |\rho_{O2s}(k, R, \eta, p_1, p_2)|.$$

Theorem 2.12 (Optimized two-sided Robin parameters)**.** *The parameter choice* $p_1^* := 2^{-\frac{5}{4}}\eta^{\frac{3}{8}}G_{\min}^{\frac{3}{4}}R^{-\frac{1}{4}}k_{\max}^{\frac{1}{4}}$ *and* $p_2^* := 2^{\frac{1}{4}}\eta^{\frac{1}{8}}G_{\min}^{\frac{1}{4}}R^{-\frac{3}{4}}k_{\max}^{\frac{3}{4}}$ *represents an asymptotic solution of the equi-oscillation problem*

$$(2.30) \quad \rho_{O2s}(k_{\min}, R, \eta, p_1^*, p_2^*) = -\rho_{O2s}(\bar{k}^*, R, \eta, p_1^*, p_2^*) = \rho_{O2s}(k_{\max}, R, \eta, p_1^*, p_2^*),$$

where $\bar{k}^* := 2^{-\frac{1}{2}}\eta^{\frac{1}{4}}G_{\min}^{\frac{1}{2}}R^{\frac{1}{2}}k_{\max}^{\frac{1}{2}}$ *represents the unique interior minimum point of* $\rho_{app}(k, R, \eta, p_1^*, p_2^*, 0, 0)$.

Proof. First, we solve the derivative of $\rho_{app}(k, R, \eta, p_1, p_2, 0, 0)$ w.r.t. k equal to zero and obtain as the unique positive solution $\bar{k} = \bar{k}(R, \eta, p_1, p_2) := \sqrt{p_1 p_2 - \eta}R$. We then make the ansatz $p_1 := C_1 k_{\max}^{\frac{1}{4}}$ and $p_2 := C_2 k_{\max}^{\frac{3}{4}}$. Inserting this ansatz into $\bar{k}$ and expanding for $k_{\max}$ large, we find $\bar{k} = \sqrt{C_1 C_2}R k_{\max}^{\frac{1}{2}} + O(k_{\max}^{-\frac{1}{2}})$. Inserting

the same ansatz into $\rho_{O2s}(k_{\min}, R, \eta, p_1, p_2)$ and expanding for $k_{\max}$ large we get

$$(2.31) \qquad \rho_{O2s}(k_{\min}, R, \eta, p_1, p_2) = 1 - \frac{\eta^{\frac{1}{2}} G_{\min}}{C_1} k_{\max}^{-\frac{1}{4}} + O(k_{\max}^{-\frac{1}{2}}).$$

Doing the same at $k = \bar{k}$ in the approximate convergence factor, we find

$$(2.32) \qquad -\rho_{app}(\bar{k}, R, \eta, p_1, p_2, 0, 0) = 1 - 4\sqrt{\frac{C_1}{C_2}} k_{\max}^{-\frac{1}{4}} + O(k_{\max}^{-\frac{1}{2}}).$$

Now using Theorem 2.4, we see that $-\rho_{O2s}(\bar{k}, R, \eta, p_1, p_2)$ has the same asymptotic expansion (2.32). Similarly, we obtain at $k = k_{\max}$:

$$(2.33) \qquad \rho_{app}(k_{\max}, R, \eta, p_1, p_2, 0, 0) = 1 - 2C_2 R k_{\max}^{-\frac{1}{4}} + O(k_{\max}^{-\frac{1}{2}}),$$

and again Theorem 2.4 shows that also $\rho_{O2s}(k_{\max}, R, \eta, p_1, p_2)$ has the expansion (2.33). Since (2.30) holds for any $k_{\max}$ large, we set the coefficients of the term $k_{\max}^{-\frac{1}{4}}$ in (2.31), (2.32) and (2.33) equal and obtain the equation

$$(2.34) \qquad \frac{\eta^{\frac{1}{2}} G_{\min}}{C_1} = 4\sqrt{\frac{C_1}{C_2}} = 2C_2 R.$$

Denoting by $C_1^* := 2^{-\frac{5}{4}} \eta^{\frac{3}{8}} G_{\min}^{\frac{3}{4}} R^{-\frac{1}{4}}$ and $C_2^* := 2^{\frac{1}{4}} \eta^{\frac{1}{8}} G_{\min}^{\frac{1}{4}} R^{-\frac{3}{4}}$ the solution of (2.34), we find p_1^*, p_2^* and $\bar{k}^*$ as announced in the theorem. $\qquad \square$

Remark 2.13. From the proof of Theorem 2.12, we see that swapping the parameters p_1^* and p_2^* does not affect the asymptotic results.

Theorem 2.14 (O2s asymptotics). *The parameters p_1^* and p_2^* given in Theorem 2.12 solve asymptotically the min-max problem (2.29). The corresponding convergence factor satisfies for $k_{\max} \to +\infty$:*

$$(2.35) \qquad \max_{k \in \mathbb{K}} |\rho_{O2s}(k, R, \eta, p_1^*, p_2^*)| = 1 - 2^{\frac{5}{4}} \eta^{\frac{1}{8}} G_{\min}^{\frac{1}{4}} R^{\frac{1}{4}} k_{\max}^{-\frac{1}{4}} + O(k_{\max}^{-\frac{1}{2}}).$$

Proof. Using similar techniques as in the proof of Theorem 2.11, we can show that $|\rho_{O2s}(k, R, \eta, p_1^*, p_2^*)|$ has local maxima at $k_{\min}$, $\bar{k}_1^*$ and $k_{\max}$ asymptotically. We then show that if $(p_1, p_2) \neq (p_1^*, p_2^*)$, there exists a k^* such that $|\rho_{O2s}(k^*, R, \eta, p_1, p_2)| > |\rho_{O2s}(k_{\min}, R, \eta, p_1^*, p_2^*)|$. Because of Remark 2.13, we can assume without loss of generality that $\beta \geq \alpha$ and thus have to investigate the following cases:

a) $\alpha > \alpha^*, \beta > \alpha$. In this case, at $k^* = k_{\min}$ we have $|\rho_{O2s}(k^*, R, \eta, p_1, p_2)| = 1 - \sqrt{\eta} \frac{G_{\min}}{C_1} k_{\max}^{-\alpha} + o(k_{\max}^{-\alpha})$.

b) $\beta = \alpha > \alpha^*$. In this case, at $k^* = k_{\min}$ we have $|\rho_{O2s}(k^*, R, \eta, p_1, p_2)| = 1 - \sqrt{\eta} G_{\min}(\frac{1}{C_1} + \frac{1}{C_2}) k_{\max}^{-\alpha} + o(k_{\max}^{-\alpha})$.

c) $\alpha \leq \alpha^*, \beta \geq \beta^*$ but $(\alpha, \beta) \neq (\alpha^*, \beta^*)$. In this case, at $k^* = C_k k_{\max}^{\frac{\alpha+\beta}{2}}$ we have, using Theorem 2.4, that $|\rho_{O2s}(k^*, R, \eta, p_1, p_2)| = 1 - 2(\frac{C_1 R}{C_k} + \frac{C_k}{R C_2}) k_{\max}^{-\frac{\beta-\alpha}{2}} + o(k_{\max}^{-\frac{\beta-\alpha}{2}})$.

d) $\alpha \leq \alpha^*, \alpha < \beta < \beta^*$. In this case, by Theorem 2.4 we have at $k^* = k_{\max}$ that $|\rho_{O2s}(k^*, R, \eta, p_1, p_2)| = 1 - 2C_2 R k_{\max}^{\beta-1} + o(k_{\max}^{\beta-1})$.

e) $\beta = \alpha < \alpha^*$. We take $k^* = k_{\max}$ in this case. Using Theorem 2.4 we obtain that $\rho_{O2s}(k^*, R, \eta, p_1, p_2) = 1 - 2(C_1 + C_2) R k_{\max}^{\alpha-1} + o(k_{\max}^{\alpha-1})$.

In each of these cases, we see that at k^* the convergence factor $|\rho_{O2s}(k, R, \eta, p_1, p_2)|$ behaves asymptotically like $1 - Ck_{\max}^{-\delta}$ with $\delta > \frac{1}{4}$ and thus the performance is worse.

It remains to study the case $(\alpha, \beta) = (\alpha^*, \beta^*)$, but $(C_1, C_2) \neq (C_1^*, C_2^*)$. If $C_1 > C_1^*$, we have from (2.31) that $|\rho_{O2s}(k_{\min}, R, \eta, p_1, p_2)| > |\rho_{O2s}(k_{\min}, R, \eta, p_1^*, p_2^*)|$ as $k_{\max} \to +\infty$. If $C_2 < C_2^*$, we have from (2.33) that $|\rho_{O2s}(k_{\max}, R, \eta, p_1, p_2)| > |\rho_{O2s}(k_{\max}, R, \eta, p_1^*, p_2^*)|$ as $k_{\max} \to +\infty$. If $C_1 < C_1^*$ and $C_2 > C_2^*$, we have from (2.32) that $|\rho_{O2s}(\bar{k}, R, \eta, p_1, p_2)| > |\rho_{O2s}(\bar{k}^*, R, \eta, p_1^*, p_2^*)|$ as $k_{\max} \to +\infty$.

Finally, the asymptotic convergence factor estimate is obtained by inserting the optimized parameters $p_{1,2}^*$ into (2.31). $\qquad\square$

Remark 2.15. If one has different values of η in different subdomains, for example η_1 in Ω_1 and η_2 in Ω_2, the analysis in this section still holds: one only needs to replace the frequently occurring term $\sqrt{\eta}G_{\min}$ by $\sqrt{\eta_1}w_k(\sqrt{\eta_1}R) - \sqrt{\eta_2}v_k(\sqrt{\eta_2}R)$ to represent the optimized transmission parameters and the corresponding estimates for the convergence factors.

3. STRAIGHT INTERFACE ANALYSIS REVISITED

We now compare the asymptotically optimized transmission parameters we obtained with those from the straight interface analysis in [18], which we will denote by a subscript "l". In the straight interface analysis, the frequency k_l is the Fourier frequency along the interface, which is connected to our analysis by the equation

$$(3.1) \qquad k_l = k/R.$$

We compare first the Taylor transmission conditions. With the frequency relation (3.1), it is easy to show that the Taylor transmission conditions of order 0 and 2 from the straight interface analysis correspond to choosing $p_i = \sqrt{\eta}, q_i = 0$ and $p_i = \sqrt{\eta}, q_i = \frac{1}{2\sqrt{\eta}R}$ in our analysis. In fact, these parameter choices can also be obtained directly by Taylor expanding the approximately optimal symbols $\sigma_i^{app}(k) = \sqrt{\eta + \frac{k^2}{R^2}} = \sqrt{\eta} + \frac{k^2}{2\sqrt{\eta}R} + O(k^4)$, where $\sigma_i^{app}(k)$ gives an identically zero approximate convergence factor ρ_{app}. They lead to the Schwarz method with approximate Taylor transmission condition of order 0 (AT0) and of order 2 (AT2) (see [28]), with corresponding convergence factors

$$(3.2) \qquad \rho_{AT0}(k, R, \eta) = \frac{-v_k(\sqrt{\eta}R) - 1}{w_k(\sqrt{\eta}R) + 1} \cdot \frac{w_k(\sqrt{\eta}R) - 1}{-v_k(\sqrt{\eta}R) + 1}$$

and

$$(3.3) \quad \rho_{AT2}(k, R, \eta) = \frac{-\sqrt{\eta}v_k(\sqrt{\eta}R) - \sqrt{\eta} - \frac{k^2}{2\sqrt{\eta}R}}{\sqrt{\eta}w_k(\sqrt{\eta}R) + \sqrt{\eta} + \frac{k^2}{2\sqrt{\eta}R}} \cdot \frac{\sqrt{\eta}w_k(\sqrt{\eta}R) - \sqrt{\eta} - \frac{k^2}{2\sqrt{\eta}R}}{-\sqrt{\eta}v_k(\sqrt{\eta}R) + \sqrt{\eta} + \frac{k^2}{2\sqrt{\eta}R}}.$$

A comparison with $\rho_{T0}(k, R, \eta)$ is shown in Figure 3.

Theorem 3.1 (Approximate Taylor asymptotics). *The parallel Schwarz method* (1.4) *with approximate Taylor transmission conditions of order* 0 *and* 2 *satisfies for* $k_{\max} \to +\infty$ *the asymptotic convergence factor estimate*

$$\max_{0 \le k \le k_{\max}} |\rho_{AT0}(k, R, \eta)| = 1 - 4\sqrt{\eta}Rk_{\max}^{-1} + O(k_{\max}^{-2}),$$

$$\max_{0 \le k \le k_{\max}} |\rho_{AT2}(k, R, \eta)| = 1 - 8\sqrt{\eta}Rk_{\max}^{-1} + O(k_{\max}^{-2}).$$

TABLE 1. Optimized transmission parameters obtained from both the circular domain analysis and the straight interface analysis.

Type	Circular domain analysis		Straight interface analysis	
OOO	$p_1 = 2^{-\frac{1}{2}}\eta^{\frac{1}{4}}G_{\min}^{\frac{1}{2}}R^{-\frac{1}{2}}k_{\max}^{\frac{1}{2}}, \quad p_2 = p_1$		$p_1 = (k_{\min,l}^2 + \eta)^{\frac{1}{4}}k_{\max,l}^{\frac{1}{2}}, \quad p_2 = p_1$	
	$q_1 = q_2 = 0$		$q_1 = q_2 = 0$	
OO2	$p_1 = 2^{-\frac{5}{4}}\eta^{\frac{3}{8}}G_{\min}^{\frac{3}{4}}R^{-\frac{1}{4}}k_{\max}^{\frac{1}{4}}, \quad p_2 = p_1$		$p_1 = 2^{-\frac{1}{2}}(k_{\min,l}^2 + \eta)^{\frac{3}{8}}k_{\max,l}^{\frac{1}{4}}, \quad p_2 = p_1$	
	$q_1 = 2^{-\frac{1}{4}}\eta^{-\frac{1}{8}}G_{\min}^{-\frac{1}{4}}R^{-\frac{5}{4}}k_{\max}^{-\frac{3}{4}}, \quad q_2 = q_1$		$q_1 = 2^{-\frac{1}{2}}(k_{\min,l}^2 + \eta)^{-\frac{1}{8}}k_{\max,l}^{-\frac{3}{4}}, \quad q_2 = q_1$	
O2s	$p_1 = 2^{-\frac{5}{4}}\eta^{\frac{3}{8}}G_{\min}^{\frac{3}{4}}R^{-\frac{1}{4}}k_{\max}^{\frac{1}{4}}, \quad q_1 = 0$		$p_1 = 2^{-\frac{1}{2}}(k_{\min,l}^2 + \eta)^{\frac{3}{8}}k_{\max,l}^{\frac{1}{4}}, \quad q_1 = 0$	
	$p_2 = 2^{\frac{1}{4}}\eta^{\frac{1}{8}}G_{\min}^{\frac{1}{4}}R^{-\frac{3}{4}}k_{\max}^{\frac{3}{4}}, \quad q_2 = 0$		$p_2 = 2^{\frac{1}{2}}(k_{\min,l}^2 + \eta)^{\frac{1}{8}}k_{max,l}^{\frac{3}{4}}, \quad q_2 = 0$	

Proof. Similar to Theorem 2.5, it is easy to prove that the convergence factors ρ_{AT0} and ρ_{AT2} are strictly increasing in k for $k > 0$. However, since for fixed $x > 0$ we know that $I_k(x)$ increases in k for $k > 0$ and $K_k(x)$ decreases in k for $k > 0$ [1], we obtain $\rho_{AT0}(0, R, \eta) = \rho_{AT2}(0, R, \eta) = \frac{K_1(\sqrt{\eta}R) - K_0(\sqrt{\eta}R)}{K_1(\sqrt{\eta}R) + K_0(\sqrt{\eta}R)} \cdot \frac{I_1(\sqrt{\eta}R) - I_0(\sqrt{\eta}R)}{I_1(\sqrt{\eta}R) + I_0(\sqrt{\eta}R)} < 0$. Thus the values of ρ_{AT0} and ρ_{AT2} at $k = 0$ can be negative, and hence ρ_{AT0} and ρ_{AT2} could attain their maxima at $k_{\min}$ or $k_{\max}$. Note however that the value of ρ_{AT0} and ρ_{AT2} at $k = 0$ is a constant. Using Lemma 2.1 we see that the convergence factors ρ_{AT0} and ρ_{AT2} tend to 1 as $k_{\max} \to +\infty$, and therefore, both ρ_{AT0} and ρ_{AT2} will eventually attain their maxima at $k_{\max}$ for $k_{\max}$ large enough. Thus, the result follows from the Taylor expansion of ρ_{app} at $k_{\max}$ and using Theorem 2.4. $\qquad \square$

Remark 3.2. The previous discussion was for $R > 0$ fixed. If R varies, the situation is different: when R is large, we see from [28] that the Taylor condition of order 0 behaves like its approximation AT0, and the latter can be obtained by a microlocal analysis. When $R \to 0$, the Schwarz algorithm with Taylor condition of order 0 behaves better than the one with the AT0 condition, since $G_0(\sqrt{\eta}R) \to \infty$ as $R \to 0$. Note that for $R > 0$ small,

$$(3.4) \qquad \frac{K_1(\sqrt{\eta}R)}{K_0(\sqrt{\eta}R)} = \frac{1}{-\ln\frac{\sqrt{\eta}R}{2} - \gamma}\frac{1}{\sqrt{\eta}R} + O(R)$$

and

$$(3.5) \qquad \frac{I_1(\sqrt{\eta}R)}{I_0(\sqrt{\eta}R)} = \frac{\sqrt{\eta}R}{2} + O(R^3),$$

where $\gamma = 0.5772156649\ldots$ is Euler's constant. Thus $\rho_{AT0}(0, R, \eta) = \rho_{AT2}(0, R, \eta) \to -1$ as $R \to 0$. To guarantee that the convergence factor at $k_{\max}$ is larger than its value at $k_{\min}$, i.e. the corresponding Schwarz method attains its asymptotic regime, $k_{\max}$ would have to be very large. Thus, when R is small, the angular mesh would need to be very fine to observe the asymptotic regime described in Theorem 3.1, since $k_{\max}$ behaves like π/h.

We next compare the optimized transmission conditions; see Table 1. Using (3.1), we see that it suffices to study the difference between $2^{-1}\eta^{\frac{1}{2}}G_{\min}$ and $\sqrt{k_{\min,l}^2 + \eta}$: if we can show that there is only a small difference, we have proved that the straight interface analysis works well for circular domain decomposition. Therefore, we
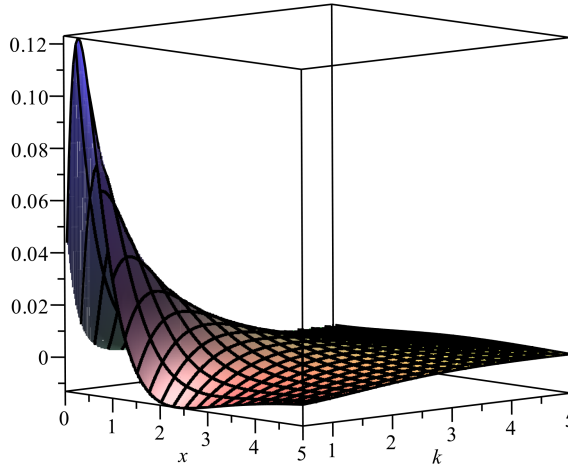
FIGURE 4. Plot of the function $f_k(x)$.

consider the relative difference $\frac{2^{-1}\eta^{\frac{1}{2}}G_{\min}-\sqrt{k_{\min,l}^2+\eta}}{2^{-1}\eta^{\frac{1}{2}}G_{\min}}$ with varying R, which means we have to study $f_k(x) := \frac{xG_k(x)-2\sqrt{k^2+x^2}}{xG_k(x)}$, for $x > 0$, evaluated at $k = k_{\min}$, since $k_{\min,l} = k_{\min}/R$. Note that $k_{\min} > 1/2$ for circular sectors and circular domains. By direct calculation, we find $f_{\frac{1}{2}}(x) = 1 - \frac{\sqrt{1+4x^2}}{x}\frac{1-e^{-2x}}{2}$, and it is easy to check that $f_{\frac{1}{2}}(x)$ attains its unique maximum 0.1231 at 0.3110 and its unique minimum -0.0131 at 2.3450. Thus $\max_{x>0}|f_{\frac{1}{2}}(x)| = 0.1231$. In addition, Figure 4 shows that $|f_k(x)| \leq \max_{x>0}|f_{\frac{1}{2}}(x)|$ for all $x > 0$ and $k > 1/2$. Hence the relative difference between $2^{-1}\eta^{\frac{1}{2}}G_{\min}$ and $\sqrt{k_{\min,l}^2+\eta}$ is quite small, and the transmission parameters obtained from the straight interface analysis also perform well when applied to circular domain decompositions, provided that the frequencies are appropriately scaled as shown in (3.1). This explains why in Figure 3 the convergence factors of the Schwarz method with transmission parameters from the circular interface analysis are so close to those with appropriately scaled parameters from the straight interface analysis.

Remark 3.3. The discussion above also applies to the overlapping case; i.e. the straight interface analysis can provide good approximations to the optimized transmission conditions for overlapping circular domain decompositions provided the frequencies are appropriately scaled, as indicated in (3.1). For a general interface, one can thus include the curvature locally in the optimized parameters by using the results from the straight interface analysis and the scaling (3.1) locally, and this for all types of problems, not just for the operator $\eta - \Delta$. This would however only be an approximation of course; other geometric characteristics of the interface would enter as well into the optimized parameters. For example, an analysis for elliptical domain decomposition shows that not only the curvature but also the semi-major axis and the semi-minor axis of the ellipse enter into the optimized parameters; see [30]. Therefore, optimized Schwarz methods with general interfaces still need to be further investigated.

TABLE 2. Number of iterations required by the optimized Schwarz methods with different transmission conditions from the circular interface analysis, when used as both direct solvers and preconditioners, compared to those (in parentheses) from the straight interface analysis [18] with the frequencies appropriately scaled. Big annular domain.

h	$\pi/50$	$\pi/100$	$\pi/200$	$\pi/400$	$\pi/800$
Optimized Schwarz as an iterative solver					
T0	148(139)	296(282)	604(581)	1272(2k+)	2k+(2k+)
OO0	21(21)	29(29)	41(41)	58(57)	82(81)
OO2	6(6)	7(7)	9(9)	10(10)	12(12)
O2s	13(12)	15(15)	18(18)	21(21)	27(26)
Optimized Schwarz as a preconditioner					
T0	15(16)	19(19)	25(25)	34(34)	48(48)
OO0	7(7)	8(8)	10(10)	11(11)	13(13)
OO2	4(4)	4(5)	5(5)	5(5)	5(6)
O2s	6(6)	7(7)	8(8)	8(8)	9(9)

4. NUMERICAL EXPERIMENTS

To illustrate our theoretical results, we perform numerical experiments for our model problem (1.1) in polar coordinates on an annulus $\Omega = (R_1, R_2) \times [0, 2\pi)$, with homogeneous Dirichlet boundary conditions on $r = R_1$ and $r = R_2$. The domain Ω is decomposed into two subdomains $\Omega = \Omega_1 \cup \Omega_2$ with $\Omega_1 = (R_1, R) \times [0, 2\pi)$ and $\Omega_2 = (R, R_2) \times [0, 2\pi)$. We choose the model parameter $\eta = 2$ and use the classical five-point finite difference scheme in polar coordinates to solve the model problem in each subdomain. We simulate directly the error equations, $f = 0$, and use a random initial guess so that all the frequency components are present; see [19, end of subsection 5.1] for the importance of this choice. We show the results when the optimized Schwarz iteration is accelerated using GMRES with restart every 30 iterations, and ask for a residual reduction of $1e-6$. The equation we solve has the exact solution $u(r, \theta) = \sin(\frac{r - R_1}{R_2 - R_1}\pi)\sin(\theta)$. To investigate how well our analytical results capture the interface curvature, we perform numerical experiments for a relatively big and a relatively small domain. In the last subsection, we show numerical results when the domain Ω is decomposed into four equally wide annuli.

4.1. **Relatively big domain.** The domain decomposition parameters are $R_1 = 0.1$, $R_2 = 0.9$ and $R = 0.5$. In the radial direction, we choose a small mesh size $1/640$, to obtain an accurate result. Table 2 (here and in the rest of the paper, '2k+' means '> 2000') shows the number of iterations required by the Schwarz method with different transmission conditions to reduce the error by a factor $1e-6$. To compare, we perform the same experiments for transmission parameters from the straight interface analysis [18] with the lowest frequency appropriately scaled to $1/R$. The corresponding results are shown in parentheses in Table 2. We see that the Taylor transmission conditions from both the circular interface analysis and the straight interface analysis perform similarly and are in agreement with
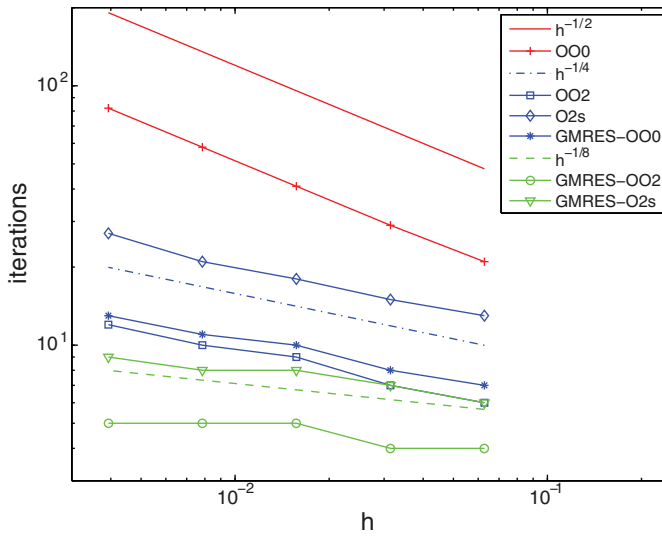
FIGURE 5. Number of iterations required by Schwarz methods with different optimized transmission conditions from our circular interface analysis, as well as those obtained by GMRES acceleration.

the theoretical prediction, requiring many iterations; the optimized transmission parameters from both analyses perform much better and about equally well. Table 2 shows in the lower part also the results when the Schwarz methods are used as preconditioners. We get a remarkable acceleration for all types of transmission conditions, but the Taylor conditions are still very much inferior compared to the optimized ones.

In Figure 5 we show a log-log plot of the number of iterations required when using the parameters from our circular interface analysis. We see that the numerical results follow well our asymptotic predictions by noting that $k_{\max} = \frac{\pi}{h}$ (see also the first paragraph of Section 2), and GMRES gives further asymptotic improvement; see also [18].

We finally investigate how well the continuous analysis predicts the optimal parameters to be used in the numerical setting. To this end, we vary the Robin parameter p with 51 samples for a fixed problem of angular mesh size $h = \pi/100$ and count for each value of p the number of iterations to reach a residual reduction of $1e - 6$, and similarly for the other transmission conditions. The results are shown in Figure 6. These results show that the analysis predicts well the optimal parameters. We also indicate in these figures the transmission parameters from the straight interface analysis ($\circ$). Appropriately scaled, they are quite close to the optimized parameters obtained from the circular interface analysis, which confirms the analysis in Section 3.

4.2. **Relatively small domain.** We now choose the domain decomposition parameters $R_1 = 0.01$, $R_2 = 0.09$ and $R = 0.05$, and take in the radial direction the mesh size to be $1/6400$. As for the relatively big domain, the number of iterations required by the Schwarz methods is shown in Table 3, when they are used as both
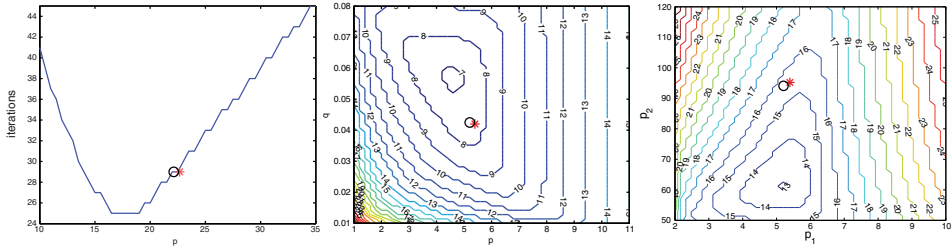
FIGURE 6. Optimized parameter (*) found by the analytical optimization compared to the optimized parameter for a straight interface (∘) reported in [18] and to the performance of other values of the parameters: from left to right for OO0, OO2 and O2s.

TABLE 3. Number of iterations required by the optimized Schwarz methods with different transmission conditions, when used as both direct solvers and preconditioners, compared to those (in parentheses) obtained using the transmission parameters from the straight interface analysis [18] with the lowest frequency properly scaled. Small annular domain.

h	$\pi/50$	$\pi/100$	$\pi/200$	$\pi/400$	$\pi/800$
Optimized Schwarz as an iterative solver					
T0	537(1443)	1124(2k+)	2k+(2k+)	2k+(2k+)	2k+(2k+)
OO0	21(21)	29(29)	41(41)	58(58)	82(82)
OO2	6(6)	7(7)	9(9)	10(10)	12(12)
O2s	13(14)	15(16)	19(18)	22(22)	27(26)
Optimized Schwarz as a preconditioner					
T0	17(17)	21(22)	26(27)	37(39)	51(53)
OO0	7(7)	8(8)	10(10)	11(11)	13(13)
OO2	4(4)	4(4)	5(5)	5(5)	6(6)
O2s	6(6)	6(6)	7(7)	8(8)	8(8)

direct solvers and preconditioners. When used as direct solvers, we see that the Taylor condition of order 0, while still satisfying the predicted asymptotic rate, is taking way too many iterations to be useful in practice. Also, the Taylor condition from the circular interface analysis performs much better than the one from the straight interface analysis, which again confirms our results from Section 3. For the optimized transmission conditions, the iteration numbers are very similar to the relatively big domain case, and this happens to be the same when the optimized Schwarz methods are used as preconditioners. Our results are thus robust with respect to the curvature parameter $1/R$.

We finally also show in Figure 7 a comparison with the numerically best performing parameters, as we did for the relatively big domain in Figure 6.

4.3. **Four-subdomain decomposition.** Equipped with the theoretical analysis and numerical tests based on bi-subdomain decomposition, we show in this subsection numerically that our optimized parameters also perform well when the computational domain is divided into many nonoverlapping subdomains. We decompose
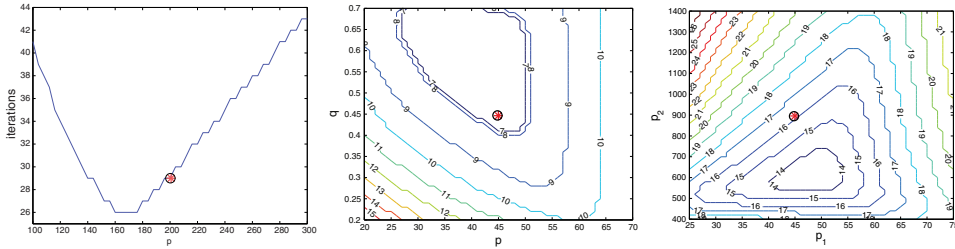
FIGURE 7. Optimized parameter (*) found by the analytical optimization compared to the optimized parameter for a straight interface (◦) reported in [6] and to the performance of other values of the parameters: from left to right for OO0, OO2 and O2s.

TABLE 4. Number of iterations required by the optimized Schwarz methods with different transmission conditions, when used as both direct solvers and preconditioners, compared to those (in parentheses) obtained using the transmission parameters from the straight interface analysis [18] with the lowest frequency properly scaled. Four-big-subdomain case.

h	$\pi/50$	$\pi/100$	$\pi/200$	$\pi/400$	$\pi/800$
Optimized Schwarz as an iterative solver					
T0	449(476)	916(960)	1902(1979)	2k+(2k+)	2k+(2k+)
OO0	87(85)	125(123)	179(175)	255(250)	363(355)
OO2	19(20)	18(18)	27(25)	35(33)	43(41)
O2s	27(25)	42(40)	58(54)	74(72)	96(92)
Optimized Schwarz as a preconditioner					
T0	49(51)	61(64)	85(89)	127(133)	212(219)
OO0	18(18)	20(20)	24(25)	29(29)	37(37)
OO2	14(14)	13(13)	12(11)	12(12)	13(13)
O2s	16(16)	16(16)	18(18)	19(19)	21(21)

the annular computational domain into four subdomains such that the boundaries form isometric concentric circles. Table 4 shows the number of iterations required by the Schwarz method with different optimized transmission conditions to reach an error reduction by a factor $1e-6$, and we also show the number of iterations required by the Schwarz method when used as a preconditioner. As in subsection 4.1, we also perform for comparison purposes the same experiments for transmission parameters from the straight interface analysis [18] with the lowest frequency properly scaled to $1/R$ with R the radius of the interface under consideration. The corresponding results are shown in Table 4 in parentheses, and they are very close to the corresponding results of our analysis. Again, in Figure 8 we show a log-log plot of iterations required when using the parameters from our circular analysis, both for the stationary iteration and as preconditioner for GMRES. We see that the numerical results also follow well our asymptotic predictions.

Similar results for the relatively small subdomain case as described in subsection 4.2 are shown in Table 5. Noting that the number of iterations shown in Table 5 is
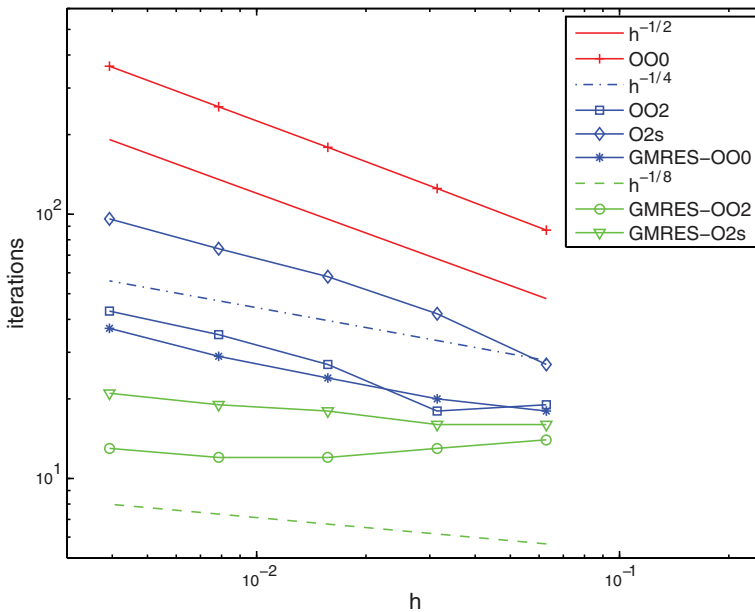
FIGURE 8. Number of iterations required by Schwarz methods
with different optimized transmission conditions from our circular
interface analysis when used as both direct solvers and precondi-
tioners. Four-big-subdomain case.

TABLE 5. Number of iterations required by the optimized Schwarz
methods with different transmission conditions, when used as both
direct solvers and preconditioners, compared to those (in parenthe-
ses) obtained using the transmission parameters from the straight
interface analysis [18] with the lowest frequency properly scaled.
Four-small-subdomain case.

h	$\pi/50$	$\pi/100$	$\pi/200$	$\pi/400$	$\pi/800$
Optimized Schwarz as an iterative solver					
T0	1333(2k+)	2k+(2k+)	2k+(2k+)	2k+(2k+)	2k+(2k+)
OO0	88(88)	129(129)	185(185)	263(263)	375(373)
OO2	24(24)	22(22)	20(21)	31(31)	40(40)
O2s	27(28)	37(36)	52(52)	70(70)	90(90)
Optimized Schwarz as a preconditioner					
T0	42(50)	52(58)	61(80)	84(95)	114(117)
OO0	15(16)	18(18)	21(21)	25(25)	30(30)
OO2	13(13)	13(13)	12(12)	10(10)	11(11)
O2s	15(15)	15(14)	15(15)	16(16)	17(17)

similar to what was found in Table 4, except for the Taylor transmission conditions,
we find that the conclusions obtained for the relatively big subdomain case remain
true and our optimized parameters are thus robust in the domain size parameter R.

5. Conclusion

We presented a complete study of optimized Schwarz methods for a nonoverlapping circular domain decomposition. Our closed form asymptotically optimal results also apply for ring shaped domains and circular sectors. We furthermore showed how to include curvature in asymptotically optimized transmission conditions from straight interface analysis by an appropriate scaling. Our numerical experiments showed that the asymptotic transmission conditions perform well and our results are robust with respect to the interface curvature. The parameters we obtained are also close to the ones performing best in the numerical setting. The small deviation is in our opinion due to the truncation to a finite domain in the numerical computation; for a preliminary study of such a truncation influence, see [29].

References

[1] M. Abramowitz and I. A. Stegun, *Handbook of mathematical functions with formulas, graphs, and mathematical tables*, National Bureau of Standards Applied Mathematics Series, vol. 55, For sale by the Superintendent of Documents, U.S. Government Printing Office, Washington, D.C., 1964. MR0167642

[2] Y. Achdou and F. Nataf, *An iterated tangential filtering decomposition*, Numer. Linear Algebra Appl. **10** (2003), no. 5-6, 511–539, DOI 10.1002/nla.326. Preconditioning, 2001 (Tahoe City, CA). MR2008372 (2004i:65110)

[3] M. Al-Khaleel, M. J. Gander, and A. E. Ruehli, *A mathematical analysis of optimized waveform relaxation for a small RC circuit*, Appl. Numer. Math. **75** (2014), 61–76, DOI 10.1016/j.apnum.2012.12.005. MR3126686

[4] M. D. Al-Khaleel, M. J. Gander, and A. E. Ruehli, *Optimization of transmission conditions in waveform relaxation techniques for RC circuits*, SIAM J. Numer. Anal. **52** (2014), no. 2, 1076–1101, DOI 10.1137/110854187. MR3198601

[5] Á. Baricz and S. Ponnusamy, *On Turán type inequalities for modified Bessel functions*, Proc. Amer. Math. Soc. **141** (2013), no. 2, 523–532, DOI 10.1090/S0002-9939-2012-11325-5. MR2996956

[6] H. Barucq, M. J. Gander, and Y. Xu, *On the influence of curvature on transmission conditions*, Domain Decomposition Methods in Science and Engineering XXI, Lecture Notes in Computational Science and Engineering 98, 2013, pp. 279–286.

[7] J.-D. Benamou and B. Desprès, *A domain decomposition method for the Helmholtz equation and related optimal control problems*, J. Comput. Phys. **136** (1997), no. 1, 68–82, DOI 10.1006/jcph.1997.5742. MR1468624 (98c:65162)

[8] D. Bennequin, M. J. Gander, and L. Halpern, *A homographic best approximation problem with application to optimized Schwarz waveform relaxation*, Math. Comp. **78** (2009), no. 265, 185–223, DOI 10.1090/S0025-5718-08-02145-5. MR2448703 (2010g:65129)

[9] E. Blayo, D. Cherel, and A. Rousseau, *Towards optimized Schwarz methods for the Navier-Stokes equations*, J. Sci. Comput. **66** (2016), no. 1, 275–295, DOI 10.1007/s10915-015-0020-9. MR3440281

[10] M. El Bouajaji, V. Dolean, M. J. Gander, and S. Lanteri, *Optimized Schwarz methods for the time-harmonic Maxwell equations with damping*, SIAM J. Sci. Comput. **34** (2012), no. 4, A2048–A2071, DOI 10.1137/110842995. MR2970396

[11] Z. Chen and X. Xiang, *A source transfer domain decomposition method for Helmholtz equations in unbounded domain*, SIAM J. Numer. Anal. **51** (2013), no. 4, 2331–2356, DOI 10.1137/130917144. MR3085122

[12] B. Després, *Décomposition de domaine et problème de Helmholtz* (French, with English summary), C. R. Acad. Sci. Paris Sér. I Math. **311** (1990), no. 6, 313–316. MR1071633 (91k:65153)

[13] V. Dolean, M. J. Gander, and L. Gerardo-Giorda, *Optimized Schwarz methods for Maxwell's equations*, SIAM J. Sci. Comput. **31** (2009), no. 3, 2193–2213, DOI 10.1137/080728536. MR2516149 (2010f:65180)

[14] V. Dolean, M. J. Gander, and E. Veneros, *Optimized schwarz methods for maxwell equations with discontinuous coefficients*, Domain Decomposition Methods in Science and Engineering XXI, Lecture Notes in Computational Science and Engineering 98, 2013, pp. 439–446.

[15] O. Dubois, *Optimized Schwarz methods for the advection-diffusion equation and for problems with discontinuous coefficients*, ProQuest LLC, Ann Arbor, MI, 2007. Thesis (Ph.D.)–McGill University (Canada). MR2711738

[16] B. Engquist and L. Ying, *Sweeping preconditioner for the Helmholtz equation: moving perfectly matched layers*, Multiscale Model. Simul. **9** (2011), no. 2, 686–710, DOI 10.1137/100804644. MR2818416 (2012i:65055)

[17] B. Engquist and H.-K. Zhao, *Absorbing boundary conditions for domain decomposition*: *Absorbing boundary conditions*, Appl. Numer. Math. **27** (1998), no. 4, 341–365, DOI 10.1016/S0168-9274(98)00019-1. MR1644668 (99j:65228)

[18] M. J. Gander, *Optimized Schwarz methods*, SIAM J. Numer. Anal. **44** (2006), no. 2, 699–731 (electronic), DOI 10.1137/S0036142903425409. MR2218966 (2007d:65121)

[19] M. J. Gander, *Schwarz methods over the course of time*, Electron. Trans. Numer. Anal. **31** (2008), 228–255. MR2569603 (2011a:65440)

[20] M. J. Gander, M. Al-Khaleel, and A. E. Ruchli, *Optimized waveform relaxation methods for longitudinal partitioning of transmission lines*, IEEE Trans. Circuits Syst. I. Regul. Pap. **56** (2009), no. 8, 1732–1743, DOI 10.1109/TCSI.2008.2008286. MR2722279 (2011e:94250)

[21] M. J. Gander and O. Dubois, *Optimized Schwarz methods for a diffusion problem with discontinuous coefficient*, Numer. Algorithms **69** (2015), no. 1, 109–144, DOI 10.1007/s11075-014-9884-2. MR3339213

[22] M. J. Gander and L. Halpern, *Absorbing boundary conditions for the wave equation and parallel computing*, Math. Comp. **74** (2005), no. 249, 153–176, DOI 10.1090/S0025-5718-04-01635-7. MR2085406 (2005h:65158)

[23] M. J. Gander and L. Halpern, *Optimized Schwarz waveform relaxation methods for advection reaction diffusion problems*, SIAM J. Numer. Anal. **45** (2007), no. 2, 666–697 (electronic), DOI 10.1137/050642137. MR2300292 (2008e:65291)

[24] M. J. Gander, L. Halpern, and F. Nataf, *Optimal Schwarz waveform relaxation for the one dimensional wave equation*, SIAM J. Numer. Anal. **41** (2003), no. 5, 1643–1681, DOI 10.1137/S003614290139559X. MR2035001 (2005h:65252)

[25] M. J. Gander, F. Magoulès, and F. Nataf, *Optimized Schwarz methods without overlap for the Helmholtz equation*, SIAM J. Sci. Comput. **24** (2002), no. 1, 38–60 (electronic), DOI 10.1137/S1064827501387012. MR1924414 (2003i:65124)

[26] M. J. Gander and F. Nataf, *AILU: a preconditioner based on the analytic factorization of the elliptic operator*, Numer. Linear Algebra Appl. **7** (2000), no. 7-8, 505–526, DOI 10.1002/1099-1506(200010/12)7:7/8⟨505::AID-NLA210⟩3.0.CO;2-Z. Preconditioning techniques for large sparse matrix problems in industrial applications (Minneapolis, MN, 1999). MR1800676 (2001k:65185)

[27] M. J. Gander and F. Nataf, *An incomplete LU preconditioner for problems in acoustics*, J. Comput. Acoust. **13** (2005), no. 3, 455–476, DOI 10.1142/S0218396X05002803. MR2174402 (2006d:76096)

[28] M. J. Gander and Y. Xu, *Optimized Schwarz methods for circular domain decompositions with overlap*, SIAM J. Numer. Anal. **52** (2014), no. 4, 1981–2004, DOI 10.1137/130946125. MR3246902

[29] M. J. Gander and Y. Xu, *Optimized Schwarz method with two-sided transmission conditions in an unsymmetric domain decomposition*, Domain Decomposition Methods in Science and Engineering XXII, Lecture Notes in Computational Science and Engineering 104, 2016, pp. 631–639.

[30] M. J. Gander and Y. Xu, *Optimized Schwarz methods for elliptical domain decompositions*, (2016), in preparation.

[31] G. Gigante, M. Pozzoli, and C. Vergara, *Optimized Schwarz methods for the diffusion-reaction problem with cylindrical interfaces*, SIAM J. Numer. Anal. **51** (2013), no. 6, 3402–3430, DOI 10.1137/120887758. MR3143836

[32] S. H. Lui, *A Lions non-overlapping domain decomposition method for domains with an arbitrary interface*, IMA J. Numer. Anal. **29** (2009), no. 2, 332–349, DOI 10.1093/imanum/drm011. MR2491430 (2010f:65283)

[33] S. H. Lui, *Convergence estimates for an higher order optimized Schwarz method for domains with an arbitrary interface*, J. Comput. Appl. Math. **235** (2010), no. 1, 301–314, DOI 10.1016/j.cam.2010.06.007. MR2671053 (2011k:65177)

[34] Y. Maday and F. Magoulès, *Optimized Schwarz methods without overlap for highly heterogeneous media*, Comput. Methods Appl. Mech. Engrg. **196** (2007), no. 8, 1541–1553, DOI 10.1016/j.cma.2005.05.059. MR2277037 (2007m:65127)

[35] F. Magoulès, P. Iványi, and B. H. V. Topping, *Non-overlapping Schwarz methods with optimized transmission conditions for the Helmholtz equation*, Comput. Methods Appl. Mech. Engrg. **193** (2004), no. 45-47, 4797–4818, DOI 10.1016/j.cma.2004.05.004. MR2097757 (2005e:65198)

[36] V. Martin, *An optimized Schwarz waveform relaxation method for the unsteady convection diffusion equation in two dimensions*, Appl. Numer. Math. **52** (2005), no. 4, 401–428, DOI 10.1016/j.apnum.2004.08.022. MR2112867 (2005i:65137)

[37] F. Nobile, M. Pozzoli, and C. Vergara, *Time accurate partitioned algorithms for the solution of fluid-structure interaction problems in haemodynamics*, Comput. & Fluids **86** (2013), 470–482, DOI 10.1016/j.compfluid.2013.07.031. MR3104148

[38] Z. Peng and J.-F. Lee, *Non-conformal domain decomposition method with second-order transmission conditions for time-harmonic electromagnetics*, J. Comput. Phys. **229** (2010), no. 16, 5615–5629.

[39] Z. Peng, V. Rawat, and J.-F. Lee, *One way domain decomposition method with second order transmission conditions for solving electromagnetic wave problems*, J. Comput. Phys. **229** (2010), no. 4, 1181–1197, DOI 10.1016/j.jcp.2009.10.024. MR2576244 (2010m:65290)

[40] L. Qin and X. Xu, *Optimized Schwarz methods with Robin transmission conditions for parabolic problems*, SIAM J. Sci. Comput. **31** (2008), no. 1, 608–623, DOI 10.1137/070682149. MR2460791 (2009j:65234)

[41] A. Alonso Rodríguez and L. Gerardo-Giorda, *New nonoverlapping domain decomposition methods for the harmonic Maxwell system*, SIAM J. Sci. Comput. **28** (2006), no. 1, 102–122 (electronic), DOI 10.1137/040608696. MR2219289 (2007e:78021)

[42] A. Vion and C. Geuzaine, *Double sweep preconditioner for optimized Schwarz methods applied to the Helmholtz problem*, J. Comput. Phys. **266** (2014), 171–190, DOI 10.1016/j.jcp.2014.02.015. MR3179763

[43] D. Yang, *A parallel nonoverlapping Schwarz domain decomposition method for elliptic interface problems*, Tech. Report IMA preprint 1508, University of Minnesota, 1997.

Section de Mathématiques, Université de Genève, 2-4 rue du Lièvre, CP 64, CH-1211, Genève, Suisse

E-mail address: `Martin.Gander@unige.ch`

School of Mathematics and Statistics, Northeast Normal University, Changchun 130024, People's Republic of China

E-mail address: `yxxu@nenu.edu.cn`